Theoretical comparison of the sensitivity of molecular contrast optical coherence tomography techniques

Brian E. Applegate, Changhuei Yang*, and Joseph A. Izatt

Department of Biomedical Engineering, Duke University, Durham, NC 27708
*current address: Department of Electrical Engineering, California Institute of Technology. Pasadena, CA 91125

brian.applegate@duke.edu, chyang@caltech.edu, jizatt@duke.edu

Abstract: Molecular contrast optical coherence tomography (MCOCT) is an extension of OCT in which contrast resulting from the interaction of light with a contrast agent, leads to the enhanced visualization of a specific morphology or biochemical process in a target specimen. In order to improve the sensitivity and specificity of MCOCT, several spectroscopic techniques have recently been introduced which depend upon coherent detection of scattered light which has been modified by interaction with the molecules of interest in a sample. These techniques include harmonic generation, coherent anti-Stokes Raman scattering, linear absorption, and several different forms of pump-probe spectroscopy. We have developed a theoretical framework to facilitate the comparison of the sensitivity of different MCOCT techniques. This framework is based upon the observation that since the noise floor is defined by the reference field power in a shot-noise limited OCT system, the relevant comparison among the techniques is isolated to the available molecular contrast signal power and the algorithm used to extract the signal. We have derived theoretical expressions for the signal power and signal-to-noise ratio for the MCOCT techniques described in the literature based on molecular spectroscopy, as well as several new techniques introduced here.

OCIS codes: (110.4500) Optical coherence tomography; (190.4180) Multiphoton processes

References and Links

1. S. Radhakrishnan, A. M. Rollins, J. E. Roth, S. Yazdanfar, V. Westphal, D. S. Bardenstein, J. A. Izatt, "Real-time optical coherence tomography of the anterior segment at 1310 nm," Arch. Ophthalmol. **119**, 1179-1185 (2001).
2. N. Nassif, B. Cense, B. H. Park, S. H. Yun, T. C. Chen, B. E. Bouma, G. J. Tearney, J. F. de Boer, "In vivo human retinal imaging by ultrahigh-speed spectral domain optical coherence tomography," Opt. Lett. **29**, 480-482 (2004).
3. S. A. Boppart, B. E. Bouma, M. E. Brezinski, G. J. Tearney, J. G. Fujimoto, "Imaging developing neural morphology using optical coherence tomography.," J. Neurosci. Methods **70**, 65-72 (1996), http://research.bmn.com/medline/search/results?uid=MDLN.97137646.
4. J. K. Barton, J. A. Izatt, M. D. Kulkarni, S. Yazdanfar, A. J. Welch, "Three-dimensional reconstruction of blood vessels from in vivo color Doppler optical coherence tomography images," Dermatology **198**, 355-361 (1999).
5. T. M. Yelbuz, M. A. Choma, L. Thrane, M. L. Kirby, J. A. Izatt, "Optical coherence tomography - A new high-resolution imaging technology to study cardiac development in chick embryos," Circulation **106**, 2771-2774 (2002).
6. U. Morgner, W. Drexler, F. X. K¨artner, X. D. Li, C. Pitris, E. P. Ippen, J. G. Fujimoto, "Spectroscopic optical coherence tomography," Opt. Lett. **25**, 111-113 (1999).
7. D. J. Faber, E. G. Mik, M. C. G. Aalders, T. G. van Leeuwen, "Light absorption of (oxy-)hemoglobin assessed by spectroscopic optical coherence tomography," Opt. Lett. **28**, 1436-1438 (2003).

#7900 - $15.00 USD Received 21 July 2005; revised 21 September 2005; accepted 23 September 2005

8. D. J. Faber, E. G. Mik, M. C. G. Aalders, T. G. van Leeuwen, "Toward assessment of blood oxygen saturation by spectroscopic optical coherence tomography," Opt. Lett. **30**, 1015-1017 (2005).
9. K. D. Rao, M. A. Choma, S. Yazdanfar, A. M. Rollins, J. A. Izatt, "Molecular contrast in optical coherence tomography by use of a pump-probe technique," Opt. Lett. **28**, 340-342 (2003).
10. B. E. Applegate, C. Yang, A. M. Rollins, J. A. Izatt, "Polarization resolved second harmonic generation optical coherence tomography in collagen," Opt. Lett. **29**, 2252-2254 (2004).
11. Y. Jiang, I. Tomov, Y. Wang, Z. Chen, "Second-harmonic optical coherence tomography," Opt. Lett. **29**, 1090-1092 (2004).
12. C. Vinegoni, J. S. Bredfeldt, D. L. Marks, S. A. Boppart, "Nonlinear optical coherence enhancement for optical coherence tomography," Opt. Express **12**, 331-341 (2004), http://www.opticsexpress.org/abstract.cfm?URI=OPEX-12-2-331.
13. J. S. Bredfeldt, C. Vinegoni, D. L. Marks, S. A. Boppart, "Molecularly sensitive optical coherence tomography," Opt. Lett. **30**, 495-497 (2005).
14. A. L. Oldenburg, F. J.-J. Toublan, K. S. Suslick, A. Wei, S. A. Boppart, "Magnetomotive contrast for in vivo optical coherence tomography," Opt. Express **13**, 6597-6614 (2005), http://www.opticsexpress.org/abstract.cfm?URI=OPEX-13-17-6597.
15. T. M. Lee, A. L. Oldenburg, S. Sitafalwalla, D. L. Marks, W. Luo, F. J.-J. Toublan, K. S. Suslick, S. A. Boppart, "Engineered Microsphere Contrast Agents for Optical Coherence Tomography," Opt. Lett. **28**, 1546-1548 (2003).
16. J. Chen, F. Saeki, B. J. Wiley, H. Cang, M. J. Cobb, Z.-Y. Li, L. Au, H. Zhang, M. B. Kimmey, X. D. Li, Y. Xia, "Gold Nanocages: Bioconjugation and Their Potential Use as Optical Imaging Contrast Agents," Nano Lett. **5**, 473-477 (2005).
17. M. A. Choma, M. V. Sarunic, C. Yang, J. A. Izatt, "Sensitivity advantage of swept-source and Fourier-domain optical coherence tomography," Opt. Express **11**, 2183-2189 (2003), http://www.opticsexpress.org/abstract.cfm?URI=OPEX-11-18-2183.
18. R. G. Byer, "Parametric oscillators and nonlinear materials"' In *Nonlinear Optics*, P. G. Harper,B. S. Wherrett, Eds. (Academic: London, 1977).
19. R. W. Boyd, *Nonlinear Optics.* (Academic: San Diego, CA, 1992).
20. P. Stoller, P. M. Celliers, K. M. Reiser, A. M. Rubenchik, "Quantitative Second-Harmonic Generation Microscopy in Collagen," Appl. Optics **42**, 5209 (2003).
21. W. Mohler, A. C. Millard, P. J. Campagnola, "Second Harmonic Generation Imaging of Endogenous Structural Proteins," Methods **29**, 97-109 (2003).
22. D. L. Marks, S. A. Boppart, "Nonlinear InterferometricVibrational Imaging," Phys. Rev. Lett. **92**, 1239051-1239054 (2004).
23. H.-o. Hamaguchi, "Nonlinear Raman Spectroscopy"' In *Nonlinear Spectroscopy for Molecular Structure Determination*, R. W. Field, E. H. A. J. P. Maier,S. Tsuchiya, Eds. (Blackwell Science, Ltd: Malden, MA, 1998).
24. A. Owyoung, P. S. Peercy, "Precise Characterixation of the Raman nonlinearity in benzene using nonlinear interferometry," J. Appl. Physics **48**, 674-677 (1977).
25. P. F. Tian, W. S. Warren, "Ultrafast measurement of two-photon absorption by loss modulation," Opt. Lett. **27**, 1634--1636 (2002).
26. A. A. Heikal, S. T. Hess, W. W. Webb, "Multiphoton molecular spectroscopy and excited-state dynamics of enhanced green fluorescent protein (EGFP): acid-base specificity," Chem. Phys. **274**, 37-55 (2001).
27. D. R. Larson, W. R. Zipfel, R. M. Williams, S. W. Clark, M. P. Bruchez, F. W. Wise, W. W. Webb, "Water-soluble quantum dots for multiphoton fluorescence imaging in vivo," Science **300**, 1434--1436 (2003).
28. C. Yang, L. E. L. McGuckin, J. D. Simon, M. A. Choma, B. E. Applegate, J. A. Izatt, "Spectral triangulation molecular contrast optical coherence tomography with indocyanine green as the contrast agent," Opt. Lett. **29**, 2016-2018 (2004).
29. M. L. J. Landsman, G. Kwant, G. A. Mook, W. G. Zijlstra, "Light- absorbing properties, stability, and spectral stabilization of indocyanine green," J. Appl. Physiol. **40**, 575-583 (1976).
30. S. Reindl, A. Penzkofer, "Triplet quantum yield determination by picosecond laser double-laser fluorescence excitation," Chem. Phys. **213**, 429-438 (1996).
31. J. I. Steinfeld, J. S. Francisco, W. L. Hase, *Chemical Kinetics and Dynamics.* (Prentice-Hall, Inc.: Englewood Cliffs, NJ, 1989).
32. S. Delysse, J.-M. Nunzi, C. Scala-Valero, "Picosecond optical Kerr ellipsometry determination of S_1-S_n absorption spetra of xanthene dyes," Appl. Phys. B **66**, 439-444 (1998).
33. J. Barroso, A. Costela, I. Garcia-Moreno, R. Sastre, "Wavelength dependence of the nonlinear absorption properties of laser dyes in solid and liquid solutions," Chem. Phys. **238**, 257-272 (1998).
34. N. Srinivas, V. Rao, N. Rao, "Saturable and reverse saturable absorption of Rhodamine B in methanol and water," J. Opt. Soc. Am. B **20**, 2470-2479 (2003).
35. C. Tanielian, C. Wolff, "Determination of the Parameters Controlling Singlet Oxygen Production via Oxygen and Heavy-Atom Enhancement of Triplet Yields," J. Phys. Chem. **99**, 9831-9837 (1995).

#7900 - $15.00 USD Received 21 July 2005; revised 21 September 2005; accepted 23 September 2005

36. B. E. Applegate, J. A. Izatt, Department of Biomedical Engineering, Duke University, Durham, NC 27708, are preparing a manuscript to be called "Transient Absorption and Lifetime Imaging with Ground State Recovery Pump-Probe Optical Coherence Tomography."
37. C. Yang, M. A. Choma, L. E. Lamb, J. D. Simon, J. A. Izatt, "Protein-based molecular contrast optical coherence tomography with phytochrome as the contrast agent," Opt. Lett. **29**, 1396-1398 (2004).
38. C. Yang, "Molecular Contrast Optical Coherence Tomography: A Review," Photochem Photobiol **81**, 215-237 (2005).
39. B. Hermann, K. K. Bizheva, A. Unterhuber, B. Považay, H. Sattmann, L. Schmetterer, A. F. Fercher, W. Drexler, "Precision of extracting absorption profiles from weakly scattering media with spectroscopic time-domain optical coherence tomography," Opt. Express **12**, 1677-1688 (2004), http://www.opticsexpress.org/abstract.cfm?URI=OPEX-12-8-1677.
40. C. Xu, D. L. Marks, M. N. Do, S. A. Boppart, "Separation of absorption and scattering profiles in spectroscopic optical coherence tomography using a least-squares algorithm," Opt. Express **12**, 4790-4803 (2004), http://www.opticsexpress.org/abstract.cfm?URI=OPEX-12-20-4790.

1. Introduction

Optical coherence tomography (OCT) is a microscopic imaging technique which utilizes low coherence light sources and interferometric detection to depth resolve the variations in reflectivity of tissue morphologies. OCT has primarily been used in imaging of the anterior segment and retina of the eye, owing to its long working distance and high speed acquisition, which combats the motion artifact inherent to imaging the living eye (see for example references [1, 2]). OCT has also more recently been used in small animal imaging for developmental biology and animal models of disease (see for example references [3-5]). The complimentary optical technique of confocal microscopy has been more commonly applied to small animal imaging. However, the superior penetration depth in OCT (~2 mm) compared to confocal microscopy (~200 μm), as well as the similar spatial resolution (~1-10 μm for OCT, sub 1 μm for confocal), make OCT an attractive complementary technique. While imaging tissue morphology by measuring depth resolved reflectivity is an important function, measuring the relative concentrations of specific molecular species is of equal or greater importance, since this information provides clues to the local chemical make up and biochemistry which is not evident from simple reflectivity measurements. This function has been embodied by the molecular imaging analogues of confocal microscopy which include confocal fluorescence, two photon fluorescence, and second harmonic generation microscopy. For the multiphoton techniques the penetration depth has been extended to ~400 μm, while confocal fluorescence remains at ~200 μm with a spatial resolution of sub 1 μm. The development of the molecular imaging analogues of OCT, collectively dubbed molecular contrast optical coherence tomography (MCOCT), holds the promise of increasing the penetration depth for molecular imaging by nearly an order of magnitude, while maintaining high spatial resolution for *in vivo* and *in situ* imaging applications.

The genesis of MCOCT has seen the development of several techniques designed to measure molecular signatures concurrent with OCT imaging. To date linear absorption (see for example references [6-8]) transient absorption[9], second harmonic generation[10, 11], and coherent anti-Stokes Raman[12, 13] spectroscopies have been demonstrated for MCOCT. Additionally, non molecular spectroscopic techniques, such as magnetomotive OCT [14] and scattering based contrast with micro-spheres have also been explored (see for example references [15, 16]). All of these molecular imaging techniques may be characterized by their sensitivity and specificity. Sensitivity is embodied by the signal to noise ratio or the related metric, minimum detectible concentration. Specificity is a measure of the ability of a technique to selectively detect the signal from a particular contrast agent on the background of signal generated by other contrast agents present in the sample. The sensitivity of a molecular spectroscopic technique may be quantifiable in terms of fundamental molecular constants of the target molecular species. Unfortunately specificity is not as easily quantified because it is dependent on the ensemble of molecular properties of

#7900 - $15.00 USD Received 21 July 2005; revised 21 September 2005; accepted 23 September 2005

the sample. For the purposes of this paper we will focus on deriving the appropriate equations to describe the sensitivity of a number of MCOCT techniques which derive their contrast from some form of molecular spectroscopy.

The traditional division of spectroscopic techniques into "dark" and "bright" field, based on whether the noise floor is defined by the signal power or some other strong field, is not apropos for the discussion of MCOCT *SNR*. This is the case because in a shot noise limited OCT system, the noise floor is always defined by the strong local oscillator. For this reason, all MCOCT techniques are bright field. Hence all MCOCT techniques are on equal footing with respect to the noise term in the *SNR* equation. It is not intuitively obvious if the dark field techniques which have an *SNR* advantage in direct detection will have any *SNR* advantage for MCOCT. What we need to consider is the effect on the signal and noise of any algorithm required to extract the MCOCT signal.

There are essentially two types of signals which we will be interested in, referenced and non-referenced signals. Referenced signals are those that measure a change in the sample arm power induced by some physical phenomenon which is being exploited for molecular contrast and therefore need a measure of the unchanged signal for comparison. For instance, the measurement of absorption is a referenced measurement, since the signal power without the absorber present must be known before the attenuation of that power may be measured. Non-referenced signals are those whose signal is generated only by interaction with the contrast agent, and thus do not require a reference measurement. An example of a non-referenced measurement is second harmonic generation, where the signal is generated only by interaction with media possessing a large 2nd order suspectibility and appears at twice the frequency of the incident radiation. In effect, the reference signal in non-referenced measurements is zero.

2. SNR comparison of bright/dark field and reference/non-referenced techniques

We first consider the general case of referenced and non-referenced interferometric signals before deriving specific expressions for the signal power and *SNR* of the MCOCT techniques discussed in this article. For a model system we assume the sample is a perfect reflector coated with some molecular species which is nonscattering. The power returning from the sample (P_s) may be grouped into two classes such that, $P_s = P_1 + P_2$. The first class (P_1) encompasses the photons which have been elastically scattered by the sample, but are otherwise unchanged. These photons are responsible for the conventional OCT signal. The second class of photons (P_2) has been elastically scattered, however at some point along the path inside the sample they have been changed in some measurable way by a molecular process. The coherent detection of these photons constitutes the MCOCT signal. For this general case the molecular contrast power is given by $P_2 = aP_s^n$, where a is a proportionality constant and P_s is again the power incident on the sample. The proportionality constant a and the order n will vary depending on what molecular process is being exploited.

We take the shot noise limited signal to noise ratio to be; $SNR = (S/\sigma_{noise})^2$, where S is the interferometric signal power and σ_{noise} is the standard deviation of the interferometric signal power characterizing the shot noise. For a referenced signal, P_2 cannot be directly measured, only its absence is measurable, hence the peak of the referenced interferometric signal power for a perfect reflector (R_s=1) is $2\sqrt{P_r}\sqrt{P_s - P_2}$. The molecular contrast signal is then the difference of the interferometric signal with and without the molecular species present, i.e.

$$S_r = 2\sqrt{P_r}\sqrt{P_s} - 2\sqrt{P_r}\sqrt{P_s - P_2} = 2\sqrt{P_r}\left(\sqrt{P_s} - \sqrt{P_s}\left(1 - aP_s^{n-1}\right)^{1/2}\right)$$
$$\approx 2\sqrt{P_r}\left(a/2\, P_s^{n-1/2}\right).$$

which leads to the expression for *SNR*

#7900 - $15.00 USD Received 21 July 2005; revised 21 September 2005; accepted 23 September 2005

$$SNR_r \propto \left(\frac{2\sqrt{P_r}\, a/2\, P_s^{n-1/2}}{\sqrt{2}\sqrt{P_r}} \right)^2 = \frac{a^2 P_s^{2n-1}}{2} \quad (1)$$

where we have approximated the quantity $(1-aP_s^{n-1})^{1/2}$ by its binomial expansion, truncating at the second term. The binomial expansion converges as long as aP_s^{n-1} is less than 1. Based on conservation of energy the maximum value of aP_s^{n-1} is 1, and for any real physical phenomenon which may be utilized for molecular contrast, $aP_s^{n-1} << 1$. In the final step, we have the generic *SNR* equation for a referenced interferometric signal in the shot noise limit, where the standard deviation of the interferometric signal power which characterizes the shot noise is $\sigma_{noise} \propto \sqrt{P_r}$, in the limit that the noise floor is dominated by the reference arm power. The additional factor of 2 in the denominator of eq. 1 is a result of the propogation of error from the subtraction of the two signals.

The derivation for a non referenced signal evolves similarly, with the exception that P_2 is directly measurable, to give

$$S_{nr} = 2\sqrt{P_r}\sqrt{aP_s^n}$$

$$SNR_{nr} \propto \left(\frac{2\sqrt{P_r}\sqrt{aP_s^n}}{\sqrt{P_r}} \right)^2 = 4aP_s^n \,. \quad (2)$$

Since a is typically much less than 1 for nonlinear processes, $SNR_{nr} > SNR_r$, for reasonable values of P_s.

It is interesting to compare the above results, to the results obtained for bright and dark field direct detection methods. By direct detection we mean in the absence of a local oscillator or non-interferometric. For bright field detection the signal and *SNR* are given by

$$S_b = P_s - \left(P_s - aP_s^n\right), \text{ and}$$

$$S_b = aP_s^n$$

$$SNR_b \propto \left(\frac{aP_s^n}{\sqrt{2}\sqrt{P_s}} \right)^2 = \frac{a^2 P_s^{2n-1}}{2}, \quad (3)$$

where, as in the referenced interferometric derivation, S_b is the signal observed as a difference in measurements taken with and without the molecular species present. Similarly, the dark field signal and *SNR* are given by

$$S_d = aP_s^n, \text{ and}$$

$$SNR_d \propto \left(\frac{aP_s^n}{\sqrt{aP_s^n}} \right)^2 = aP_s^n \,. \quad (4)$$

A comparison of Eqs. (1) to (3) and (2) to (4), reveals that interferometric referenced *SNR* is approximately equivalent to direct detection bright field *SNR*, and non-referenced interferometric *SNR* is approximately equivalent to dark field *SNR*. In principle the properties of the electromagnetic radiation which allow for the separation of the input radiation from the signal radiation in direct detection are the same as those which would allow for non-referenced interferometric detection. Therefore any signal that is bright field in direct detection must also be a referenced signal in interferometric detection and likewise for non-referenced interferometric and dark field.

#7900 - $15.00 USD Received 21 July 2005; revised 21 September 2005; accepted 23 September 2005

The superiority of dark field and non-referenced signal to noise over the alternatives is illustrated in Fig. 1. Figure 1 is a plot of Eqs. (3) and (4) with units of power such that P_s=1. Under this condition, $a \le 1$. Clearly for all values of a except the trivial case of a=0, dark field/non-referenced *SNR* is larger than bright field/referenced *SNR*. We can mathematically show the same outcome by taking the ratio of Eqs. (3) and (4). The result is

$$\frac{SNR_b}{SNR_d} = \frac{aP_s^{n-1}}{2} \le 1/2. \tag{5}$$

where as before the final inequality is a result of the principle of conservation of energy. It follows then from Eq. (5) that $SNR_d \ge 2SNR_b$.

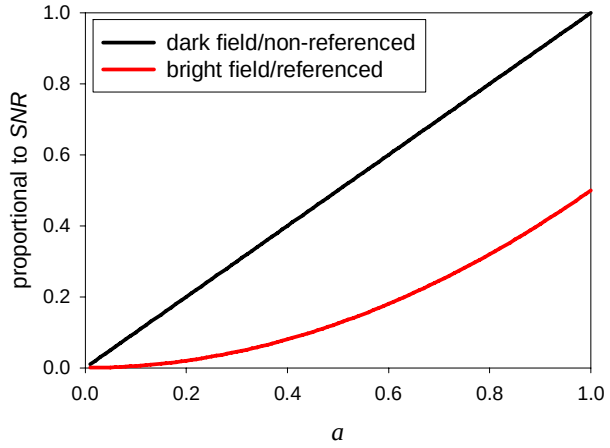

Fig. 1 Plot of eqns (3) and (4) with units of power such that P_s=1, which implies that $a \le 1$.

While we have clearly shown above the superiority of dark field detection, it is also very important to consider the strength of the interaction being used for contrast. As we will show later in this article, bright field techniques which utilize strong molecular processes (i.e. large a) can still have better SNR than techniques using weaker molecular processes but are dark field.

3. SNR derivation for MCOCT techniques

The signal to noise ratio of a spectral domain OCT system [17] is given by

$$SNR_{OCT} = \frac{\rho R_s \Delta t}{2e} P_s, \tag{6}$$

where ρ is the detector responsivity, R_s is the sample reflectivity, P_s is the power incident on the sample, Δt is the integration time, and e is the electron charge. The signal to noise ratio of a spectral domain MCOCT system may be defined similarly by replacing P_s in Eq. (6) by the molecular contrast signal power, P_{MCOCT}. For non-referenced techniques, P_{MCOCT} has a similar physical meaning to P_s, and is exactly equal to P_2. For referenced techniques, P_{MCOCT} is modified to include the effects of multiple measurements, which in addition to P_2 includes any affect on the noise term of the algorithm used to extract P_{MCOCT}.

In the following sections we derive the molecular contrast signal power, P_{MCOCT}, and expressions for *SNR* of previously reported MCOCT techniques, as well as novel techniques which we propose here for the first time. In the sensitivity analysis of conventional OCT systems, it is customary to specify the sensitivity of the system by stating the signal to noise

#7900 - $15.00 USD Received 21 July 2005; revised 21 September 2005; accepted 23 September 2005

Table 1. Results of the derivations of expressions for P_{MCOCT} described in the text.

Technique	P_{MCOCT}		***SNR* (dB)**	**Min. Det. Con.**
	***theoretical*[b]**	***example(W)***		
SHOCT	$\frac{2\left\|\chi^{(2)}_{SHG,eff}\right\|^2}{\pi w_0^2}\frac{\omega_1^2}{n_1^2 n_2 c^3 \varepsilon_0 f_0 \tau}\left\|J\right\|^2 P_{1\omega}^2$	pure Collagen 1.49×10^{-10}	54	*c*
NIVI (CARS)	$\frac{256\pi^2\omega_{as}^2}{n_p^2 n_{st} n_{as} c^4 r^2 \tau^2 f_0^2}\left\|\chi^{(3)}_{CARS} N_1\right\|^2 l^2 \times \left[\mathrm{sinc}(\Delta k l/2)\right]^2 P_{st} P_p^2$	pure Benzene 1.94×10^{-12} Benzene 1.54×10^{-22}	36 -65	 180 mM
TPA-OCT	$\left(\frac{0.66 N_1^0 \delta n}{8\pi f_0 hc}\arctan\left(\frac{l}{n2z_0}\right)\right)^2 P_S^3$	EGFP 4.66×10^{-17} Quantum Dots 1.68×10^{-11}	-11 45	360 µM 560 nM
SOCT: Spectral Triang-ulation	$\frac{e^{-2\sigma_b Nl}\left(e^{-\sigma_b Nl(\alpha-1)}-1\right)^2}{9\left(\frac{1}{4}e^{2\mu_{s,a}l}+\frac{1}{4}e^{2\mu_{s,c}l}+e^{2\mu_{s,b}l+2\sigma_b Nl(1-\alpha)}\right)}P_s$	ICG α=0.77 6.31×10^{-8} Rhodamine 6G 3.98×10^{-8}	81 79	8.9 nM 11 nM
PPOCT[a] scheme 1	$\left(\frac{\sigma_2 l N_1^0 \sigma_1 \lambda_{pu} P_{pu}}{2hc\pi r^2 f_0}\right)^2 P_{pr}$	Rhodamine 6G 1.90×10^{-10}	56	160 nM
PPOCT[a] scheme 2 (gsrPPOCT)	$\left(\frac{\sigma_1^2 l N_1^0 \lambda_{pu} P_{pu}}{hc\pi r^2 f_0}\right)^2 P_{pr}$	Rhodamine 6G 6.25×10^{-8}	81	8.9 nM
PPOCT[a] scheme 3	$\left(\frac{\sigma_3 q_{2,3} l N_1^0 \sigma_1 \lambda_{pu} P_{pu}}{2hc\pi r^2 f_0}\right)^2 P_{pr}$	Rhodamine 6G 2.65×10^{-14}	17	14 µM

For definitions of the symbols used in the theoretical expressions see the text. Predicted values of P_{MCOCT} and *SNR* in columns 3 and 4 are for the model system noted in the text with the following parameters for all techniques: 10 mW total power on sample, 15 µm pathlength through sample, a 3.2 µm focal spot radius, detector responsivity of 0.6 A/W, and an integration time of 1 ms. Unless otherwise stated the concentration of all exogenous contrast agents was fixed at 100 µM. [a] The dependence of the PPOCT signal on f_0 is a result of treating each pulse of the laser independently. f_0 may not be arbitrarily decreased in order to increase PPOCT *SNR*, since the approximation that $1/\tau >> A$ will cease to be valid. [b] Only the expression for SHOCT and TPA-OCT specifically takes into account the effects of focusing, although all of the techniques, except spectral triangulation are sensitive to this parameter. While this does not affect the results in columns 3 and 4 of table 1 since the thickness of the model sample is well within twice the Rayleigh distance of the focused beam, it will be important for OCT systems which have not been designed with a depth of focus equal to or greater than the tissue penetration depth. For those systems, in order to gain quantitative results from the expressions, the spatial variation of the irradiance would need to be included. [c] Lacking the density and molar mass of the collagen fibrils measured, it is not possible to convert the measured bulk nonlinear susceptibility into a per molecule measurement.

#7900 - $15.00 USD Received 21 July 2005; revised 21 September 2005; accepted 23 September 2005

ratio for a perfectly reflecting sample. The analogous model system for MCOCT is a perfect reflector coated with a generic contrast agent which exhibits the phenomenon being exploited for molecular contrast. For convenience we also assume there is no scattering induced by the contrast agent. Table 1 summarizes the results of the derivations described below. The first column gives the name (or acronym, definitions below) of the technique. The second column gives the theoretical expression for P_{MCOCT}, as well as the value of P_{MCOCT} for a particular contrast agent. To evaluate P_{MCOCT} as we have for particular contrast agents, a set of conditions must be assumed. We have assumed an average power of 10 mW, a transform limited pulse length of 200 fs, a repetition rate of 72 MHz, a pathlength of 15 μm, and a beam spot radius of 3.2 μm. Other assumptions, which are specific to a technique, have been enumerated in the appropriate sections below. The final column is the expected *SNR* on system with a detector responsivity of 0.6 A/W and an integration time of 1 ms. If the entire 10 mW was in P_1, the *SNR* of the OCT system would be 133 dB. A typical tissue sample would exhibit a maximum reflectivity of ~ -50 dB, hence an OCT system with 133 dB *SNR* would have a maximum image *SNR* of ~83 dB. Likewise, for an MCOCT technique, if we predict an *SNR* of 80 dB for a perfect reflector, a tissue sample with maximum reflectivity of -50 dB would show a maximum *SNR* of 30 dB in the image.

3.1 Second Harmonic Optical Coherence Tomography

Second harmonic generation spectroscopy has recently been adapted to OCT by several groups [10-12]. We have derived P_{MCOCT} for second harmonic OCT (SHOCT) and for the more general case of sum frequency generation OCT (SFOCT). Sum frequency generation is a process by which two photons of frequency ω_1 and ω_2 are mixed in a nonlinear material to generate a third photon of frequency ω_{SFG}, which obeys the equation; $\omega_1 + \omega_2 = \omega_{SFG}$. Second harmonic generation is a special case of sum frequency generation where the two photons have the same frequency. The sum frequency power is proportional to the product of the power at the two frequencies times a proportionality constant *a*, which is a function of the 2nd order susceptibility and the number density of the contrast agent, i.e. $P_{SFG} = aP_{\omega 1}P_{\omega 2}$. SFOCT is a non-referenced technique since the signal is frequency shifted away from the OCT signal. The MCOCT power for SFOCT is then simply given by $P_{SFOCT} = aP_{\omega 1}P_{\omega 2}$, which simplifies to

$$P_{SHOCT} = aP_{\omega 1}^2 \tag{7}$$

for SHOCT. An expression for *a* has been derived previously using the theory described by Byer [18] and Boyd [19] for a Gaussian beam focused to a diffraction limited spot with 1/e radius w_0 by Rubenchik et al. [20] and is given by;

$$a = \frac{2\left|\chi^{(2)}_{SHG,eff}\right|^2}{\pi w_0^2}\frac{\omega_1^2}{n_1^2 n_2 c^3 \varepsilon_0 f_0 \tau}\left|J\right|^2, \tag{8}$$

where $\chi^{(2)}_{SHG,eff}$ is the effective 2nd order susceptibility, ω_1 is the frequency of the incident radiation, n_1 is the refractive index at the fundamental frequency, n_2 is the refractive index at the second harmonic frequency, *c* is the speed of light, ε_0 is the permittivity of free space, τ is the temporal bandwidth of the laser source, f_0 is the laser pulse repetition rate, and *J* is an integral describing the focusing and phase matching of the beam (see ref. [20] for details).

Since SHOCT has been demonstrated experimentally using both nonlinear crystals[10-12] as well as in real tissue samples[10, 11], we may compare this result to experimental measurements. Combining Eqs. (6) and (7) we find that the measured *SNR* of the fundamental should be equal to the second harmonic *SNR* divided by $aP_{\omega 1}$, assuming that the noise levels are the same for the fundamental and second harmonic. Note that this result holds even if the measurements are not shot noise limited, as long as our assumption that the

#7900 - $15.00 USD Received 21 July 2005; revised 21 September 2005; accepted 23 September 2005

noise levels for the fundamental and second harmonic are the same is still good. The experimental results in reference [10], where the authors sequentially measured the *SNR* of the fundamental and second harmonic signals, support this conclusion. They measured SNR_{OCT} =114 dB and $SNR_{SHOCT}/\ aP_{\omega 1}$=113 dB. The 1 dB discrepancy was within the experimental error. The quadratic dependence of SNR_{SHOCT} on the power of the fundamental was also demonstrated in references [10-12], thereby confirming the fundamental equation from which the SHOCT power was derived .

Collagen is the prototypical endogenous contrast agent for second harmonic generation. A recent study by Rubenchik et al. [20], which quantified the second harmonic generation of a pure collagen sample made it possible to theoretically predict P_{SHOCT} for such a sample. After substituting Eq. (8) into Eq. (7), we used the experimental conditions enumerated previously and the parameters measured in reference [20] for w_0 = 3.2 μm to calculate a P_{SHOCT} of 1.49×10^{-10} W with a corresponding *SNR* of 54 dB for our model system. This should be taken as the maximum value one might expect under these given conditions, for several reasons. No biological sample is pure collagen. We have not explicitly considered the losses due to destructive interference between second harmonic light generated at different points in the tissue. We have implicitly assumed that the laser polarization is aligned with the molecular hyperpolarizability, thereby providing the maximum second harmonic response. This latter condition has been exploited to deduce the relative orientation of the collagen fibers in a tissue sample, for SHOCT see reference [10] and for second harmonic microscopy, see for instance reference [21].

3.2 Non-linear Interferometric Vibrational Imaging

Another nonlinear spectroscopy which has recently been incorporated into OCT is coherent anti-Stokes Raman scattering, or CARS. The developers of this technique called nonlinear interferometric vibrational imaging (NIVI), have recorded an interferogram generated by the CARS emission from cuvettes filled with pure benzene. In principle NIVI has the potential to differentiate between contrast agents based upon their vibrational spectrum. However, in practice this is complicated by the requirement of spectrally broad sources in OCT which severely degrades the spectral resolution. A possible solution of this problem has been proposed theoretically in reference [22].

CARS is a four wave mixing process due to the 3rd order susceptibility in which two pump photons and the Stokes photon are mixed in the nonlinear material to generate the anti-Stokes photon. When the difference of the pump and Stokes photon is tuned to a Raman active vibrational mode, the power of the anti-Stokes photon is enhanced. The frequency of the anti-Stokes photon is given by the equation; $2\omega_p - \omega_{st} = \omega_{as}$. The CARS power is then given by $P_{CARS}=bP_p^2P_{st}$, where *b* is a proportionality constant dependent on the value of $\chi^{(3)}$ and the number density of the molecular contrast agent. An expression for the proportionality constant, *b*, may derived starting from equation 8.17 of reference [23] to get;

$$b = \frac{256\pi^2\omega_{as}^2}{n_p^2 n_{st} n_{as} c^4 r^2}\left|\chi_{CARS}^{(3)} N_1\right|^2 l^2 \left[\mathrm{sinc}(\Delta k l/2)\right]^2, \tag{9}$$

where n_p, n_{st}, and n_{as} are the refractive index of the nonlinear material at ω_p, ω_{st} and ω_{as}, respectively, *c* is the speed of light, N_1 is the molecular population of the Raman level being probed, *l* is the pathlength through the nonlinear material, Δk is the phase mismatch between the wavevectors k_p and k_{st}, and *r* is the beam spot radius. NIVI is a non–referenced technique; hence the MCOCT power is given by

$$P_{NIVI} = \frac{256\pi^2\omega_{as}^2}{n_p^2 n_{st} n_{as} c^4 r^2 \tau^2 f_0^2}\left|\chi_{CARS}^{(3)} N_1\right|^2 l^2 \left[\mathrm{sinc}(\Delta k l/2)\right]^2 P_{st} P_p^2. \tag{10}$$

#7900 - $15.00 USD Received 21 July 2005; revised 21 September 2005; accepted 23 September 2005

Unfortunately, to our knowledge, the CARS response has not been sufficiently quantified for any practical endogenous or exogenous contrast agent to allow for the theoretical calculation of the expected *SNR* as was done previously for SHOCT. However, benzene, the contrast agent which was used to first demonstrate NIVI, has been well characterized. The $\chi^{(3)}_{\mathrm{CARS}}$ for benzene was determined in 1977 in an interferometric experiment[24] very similar to the original NIVI demonstration and found to be $2.35\text{x}10^{-40}$ m^6/J . In addition to the standard conditions assumed above we also partition the 10 mW of power into P_p = 6.65 mW and P_{st} =3.35 mW, which optimizes Eq. (10) and assume a benzene concentration. We have assumed a concentration of 100 μM to simulate the concentration one might find for an exogenous contrast agent and pure liquid phase benzene ($6.757\text{x}10^{26}$ molecules/m^3) to simulate the concentration one might find for an endogenous contrast agent. Under these conditions we have found P_{NIVI} and the *SNR* for the 100 μM solution to be $1.54\text{x}10^{-22}$ W and -65 dB, respectively. For the pure benzene sample P_{NIVI} was found to be $1.94\text{x}10^{-12}$ W with the corresponding *SNR* of 36 dB.

3.3 Two-Photon Absorption Optical Coherence Tomography

We propose here a second 3rd order process, which may potentially be used for MCOCT, two photon absorption. The fluorescence analog, two photon fluorescence is commonly used for nonlinear microscopy. Two photon absorption is a resonant process whereby two photons of frequency $\omega_r/2$ are absorbed simultaneously to excite a molecule resonance at ω_r. An expression for the power absorbed via a two photon process has been derived previously[25] and is given by;

$$P_{TPA} = \xi P_s^2 = \frac{0.66 N_1^0 \delta n}{\tau f_0 h c} \arctan\left(\frac{l}{n 2 z_0}\right) P_s^2 \tag{11}$$

where $N_1{}^0$ is the ground state population, δ is the two photon absorption cross-section, n is the refractive index of the sample, τ is the pulsed duration of the source, f_0 is the repetition rate, h is Planck's constant, c is the speed of light, l is the pathlength through the sample, z_0 is the Rayleigh length, and P_s is the power incident on the sample. TPA-OCT is referenced technique because the MCOCT signal is at the same optical frequency as the incident radiation. The signal measured with the two-photon absorber in the sample is given by;

$$S = 2\sqrt{P_r}\sqrt{P_s}\left(1 - \tfrac{1}{2}\xi P_S\right). \tag{12}$$

As before we have expanded the right hand side of Eq. 12 via the binomial series, which converges as long as $|P_{TPA}/P_s|<1$ and truncated at the second term. At this point there is no physical way to separate signal contributions from (P_S) and (ξP_s) without making a measurement without the two-photon absorber present. However, if we modulate P_s, such that $P_s' = P_s \sin^2(\omega t)$, Eq. (12) becomes

$$\begin{aligned} S &= 2\sqrt{P_r}\sqrt{P_s \sin^2(\omega t)}\left(1 - \tfrac{1}{2}\xi P_S \sin^2(\omega t)\right) \\ &= 2\sqrt{P_r}\left(\left(P_S^{1/2} - \tfrac{3}{8}\xi P_S^{3/2}\right)\sin(\omega t) + \tfrac{1}{8}\xi P_S^{3/2}\sin(3\omega t)\right). \end{aligned} \tag{13}$$

where signal at the third harmonic is entirely due to the two photon absorption. Demodulation of the signal at 3ω yields;

$$S_{TPA} = \tfrac{1}{8}\xi P_S^{3/2}. \tag{14}$$

The molecular contrast power is then;

$$P_{TPA-OCT} = \left(\tfrac{1}{8}\xi\right)^2 P_S^3. \tag{15}$$

Modulation of the sample power and monitoring the two photon absorption signal at the harmonics of the modulation frequency was originally proposed and demonstrated by Tian and Warren [25], in a direct detection technique.

#7900 - $15.00 USD Received 21 July 2005; revised 21 September 2005; accepted 23 September 2005

Potential contrast agents for TPA-OCT include those used for two photon fluorescence microscopy, e.g. transfectable proteins and quantum dots, as well those two photon absorbers which do not fluoresce. As examples we have considered enhanced green fluorescent protein (EGFP) and quantum dots. While strictly speaking quantum dots are not molecules, they do posses properties which allow them to be detected in a similar way. Under the conditions enumerated earlier for EGFP with a two photon cross-section of $\delta = 75\text{x}10^{-50}$ cm^{4}s at 950 nm [26] the $P_{TPA\text{-}OCT}$ is $4.60\text{x}10^{-17}$ W, with a corresponding *SNR* of -11 dB. The 605 nm quantum dots from Quantum dot corporation have a cross-section of $\delta \sim 45{,}000\text{x}10^{-50}$ cm^{4}s between 700-1100nm[27]. This results in a significantly larger $P_{TPA\text{-}OCT}$ of $1.68\text{x}10^{-11}$ W, with a corresponding *SNR* of 45 dB.

3.4 Spectroscopic Optical Coherence Tomography- Spectral Triangulation

Spectroscopic OCT (SOCT) is a class of techniques which exploits the linear absorption of the sample arm light by molecular contrast agents. Unlike the previous three examples, P_1 and P_2 are not easily separated. Since attenuation of the sample arm power due both to scattering and absorption ostensibly obey the Beer-Lambert law, they are inseparable without taking advantage of the more distinctive wavelength dependence of the absorption coefficient (μ_a). Several techniques have been developed to extract this information. We will explicitly consider a technique recently demonstrated called spectral triangulation [28]. Spectral triangulation is based upon the assumption that the tissue scattering coefficient varies linearly across the spectral bandwidth of the source. Under this assumption, it is possible by a simple algorithm to separate the linear contributions to the attenuation from the nonlinear contributions. All of the nonlinear contributions are then attributed to absorption. With this technique, OCT images at three equally spaced wavelengths (λ_a, λ_b, and λ_c) are recorded either separately with a tunable source or simultaneously with a broadband source, and combined with the following algorithm:

$$S_{ST} = \frac{\sqrt{S(\lambda_a)S(\lambda_c)}}{S(\lambda_b)} - 1 = e^{-\left(\frac{\sigma_a+\sigma_c}{2}-\sigma_b\right)Nl} - 1 \approx e^{-\sigma_b(\alpha-1)Nl} - 1 \qquad (16)$$

where S_{ST} is the spectral triangulation signal, $S(\lambda)$ is the signal at wavelength λ, and σ, N, and l have their standard meaning from the Beer-Lambert law, i.e. absorption cross-section, molecular population and pathlength, respectively. The final approximation comes from the assumption that $\sigma_a = \sigma_c = \alpha\sigma_b$, which is tantamount to assuming that the absorption peak is symmetric and centered at λ_b. It is interesting to note that the signal in spectral triangulation is not power dependent as long as equivalent power is used at all three wavelengths. However, as seen below, the noise is power dependent. The noise term is simply the statistical propagation of the standard deviation of the shot-noise of each measurement through the algorithm above. Combining S_{ST} and the noise term we may derive the P_{SOCT} to be

$$P_{SOCT} = \frac{e^{-2\sigma_b Nl}\left(e^{-\sigma_b Nl(\alpha-1)} - 1\right)^2}{9\left(\tfrac{1}{4}e^{2\mu_{s,a}l} + \tfrac{1}{4}e^{2\mu_{s,c}l} + e^{2\mu_{s,b}l+2\sigma_b Nl(1-\alpha)}\right)} P_s, \qquad (17)$$

where $\mu_{s,a}$ is the scattering coefficient at λ_a and P_s is the total power incident on the sample. As noted before, P_{SOCT} is the quantity that is substituted into equation 6 in order to find the *SNR* equation for spectral triangulation. In the limit that $\sigma_a = \sigma_c = 0$, spectral triangulation measures the absolute magnitude of the absorption. This is of course the limit to what any spectroscopic OCT algorithm can hope to achieve.

As an example, we have considered the molecular contrast agent, indocyanine green (ICG), which was used in the original demonstration of spectral triangulation [28]. Based upon the absorption spectrum reported in the literature[29] for a 65 μM solution of ICG in

#7900 - $15.00 USD Received 21 July 2005; revised 21 September 2005; accepted 23 September 2005

water, a spectral triangulation image recorded with wavelengths 780 nm +/- 25 nm would yield an α of 0.77. If we then assume an ICG concentration of 100 μM and use the literature value for the cross-section, i.e. σ_b = 4.8x10^{-16} cm^2, the expected P_{SOCT} is 6.31x10^{-8} W with a corresponding *SNR* of 81 dB. For comparison we have also considered rhodamine 6G. If we again assume α= 0.77 and use the literature value[30] of $\sigma_{a,b}$ = 3.8x10^{-16} , P_{MCOCT} is 3.98x10^{-8} W with an *SNR* of 79 dB. In the limit that α=0, P_{SOCT} goes to 7.94x10^{-7} W and the *SNR* goes to 92 dB.

3.5 Pump-Probe Optical Coherence Tomography

The final technique we will consider is pump-probe OCT (PPOCT). Pump-probe spectroscopy was the first nonlinear technique adapted to measure molecular contrast with OCT[9]. The most basic pump-probe experiment involves pumping molecular population, via a resonant transition between two states and then probing the change in population induced by the pump beam with the probe beam, which is tuned to another molecular resonance. The only requirement is that the two molecular resonances have at least one state in common between them.

For pump-probe OCT, the derivation of P_{MCOCT} requires explicitly tracking the population changes in the states utilized in the pump-probe scheme. Here, we consider the three most prominent two-photon pump-probe schemes based on electronic transitions. These are shown graphically in Fig. 2. Higher order pump-probe schemes require multiple spontaneous processes, which will invariably lead to significant losses in the efficiency. Scheme 1 is the most common pump probe experiment, where the pump excites molecules from state 1 into state 2 and the probe interrogates the population of state 2 by monitoring the transient absorption from state 2 to state 4. Scheme 2 is a ground state recovery pump-probe approach in which the pump excites molecules from state 1 to state 2, and the probe interrogates the population of state 1 by monitoring the transient bleaching of the 1-2 transition. Scheme 3 is similar to scheme 1, except that a spontaneous process is required to transfer population from state 2 to state 3 and the population of state 3 is monitored with the 3-5 transition. The efficiency of the spontaneous process is given by the quantum efficiency, $q_{2,3}$. Scheme 3 is the technique which was utilized in the first demonstration of PPOCT in methylene blue. In methylene blue the spontaneous process which transferred population from state 2 to state 3 was a spin forbidden singlet-triplet transition.

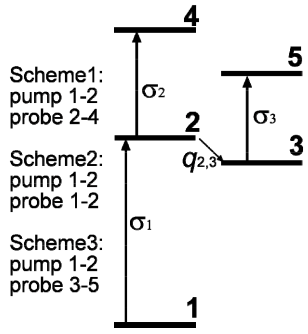

Fig. 2. Pump-probe schemes.

The maximum of the interferometric signals for each of scheme 1-3 are given by;

#7900 - $15.00 USD Received 21 July 2005; revised 21 September 2005; accepted 23 September 2005

$$S_1 = 2\sqrt{P_r}\sqrt{P_{pr}}e^{-\sigma_2 N_2(t)l}$$
$$S_2 = 2\sqrt{P_r}\sqrt{P_{pr}}e^{-\sigma_1(N_1(t)-N_2(t))l}\ , \tag{18}$$
$$S_3 = 2\sqrt{P_r}\sqrt{P_{pr}}e^{-\sigma_3 q_{2,3} N_2(t)l}$$

respectively. Where we have assumed weak absorption of the probe beam, hence the Beer-Lambert law holds, P_r is reference arm power, P_{pr} is the probe/sample arm power and $N_1(t)$ and $N_2(t)$ are the time dependent populations of states 1 and 2, respectively. If we restrict ourselves, for the pump radiation, to a two level system, the coupled differential equations which describe the time dependent populations of states 1 and 2 have a well known solution [31], namely;

$$N_1(t) = \frac{N_1^0}{2\rho B + A}\left[A + \rho B + \rho B e^{-(2\rho B + A)t}\right] \text{ and} \tag{19}$$

$$N_2(t) = N_1^0 - N_1 = \frac{\rho B N_1^0}{2\rho B + A}\left[1 - e^{-(2\rho B + A)t}\right], \tag{20}$$

where $N_1{}^0$ is the initial ground state population, ρ is the radiation density, A and B are Einstein coefficients, t is the integration time, and we have assumed that state 2 is unpopulated before interacting with the pump radiation. In the limit that the absorption cross-section is constant across the bandwidth of the radiation source,

$$\rho B = \frac{\sigma_1 \lambda_{pu} P_{pu}}{hc\pi r^2}, \tag{21}$$

where λ_{pu} is the pump wavelength, P_{pu} is the average pump power, h is Planck's constant, c is the speed of light, and r is the focal spot radius. If we restrict ourselves to pulsed radiation sources with pulse duration τ and repetition rate f_0, and assume that $A >> f_0$ then all of the population transferred in one pulse sequence of the pump and probe returns to the ground state before the next pulse sequence. Under these conditions each pump-probe pulse sequence is independent of the next and all of the relevant physics may be gleaned by considering only a single pulse sequence. In order to transform Eqs. (19) and (20) into the single sequence regime, we need only multiply Eq. (21) by the quantity $(f_0\tau)^{-1}$ before substituting for ρB to convert from average power to pulse power and substitute the pulse length τ for the integration time t. Eqs. (19) and (20) become;

$$N_1(\tau) = N_1^0\left(1 - \frac{\sigma_1 \lambda_{pu} P_{pu}}{hc\pi r^2 f_0}\right) \text{ and} \tag{22}$$

$$N_2(\tau) = N_1^0 \frac{\sigma_1 \lambda_{pu} P_{pu}}{hc\pi r^2 f_0}, \tag{23}$$

where we have taken the limit of A=0 and approximated the exponential function with its Taylor series expansion and truncated the series at the second term. These approximations are good in the limit that $A << 1/\tau$ and the pump radiation is only weakly absorbed, respectively. The peak of the interferometric signal power from a single pulse sequence for scheme 1 is then;

$$S_1' = \frac{2\sqrt{P_r}\sqrt{P_{pr}}}{f_0\tau}e^{-\sigma_2 N_2(\tau)l} \approx \frac{2\sqrt{P_r}\sqrt{P_{pr}}}{f_0\tau}(1 - \sigma_2 l N_2(\tau)), \tag{24}$$

where in the final approximation we have again approximated the exponential function with the first two terms of its Taylor series expansion. Combining Eqs. (23) and (24) we have;

#7900 - $15.00 USD Received 21 July 2005; revised 21 September 2005; accepted 23 September 2005

$$S_1' = \frac{2\sqrt{P_r}\sqrt{P_{pr}}}{f_0\tau}\left(1-\sigma_2 l N_1^0 \frac{\sigma_1\lambda_{pu}P_{pu}}{hc\pi r^2 f_0}\right) \tag{25}$$

for the peak interferometric signal for a single pulse sequence. The average signal is then product of Eq. 25 with the pulse duration τ and repetition rate f_0, to get

$$S_1 = 2\sqrt{P_r}\sqrt{P_{pr}}\left(1-\sigma_2 l N_1^0 \frac{\sigma_1\lambda_{pu}P_{pu}}{hc\pi r^2 f_0}\right). \tag{26}$$

We may separate the signal due to P_1 and P_2 by modulating the pump power by $P_{pu}' = P_{pu}\sin^2(\omega/2t)$. The signal at ω is then

$$S_1(\omega) = \sqrt{P_r}\sqrt{P_{pr}}\left(\sigma_2 l N_1^0 \frac{\sigma_1\lambda_{pu}P_{pu}}{2hc\pi r^2 f_0}\right) \text{ and} \tag{27}$$

$$P_{PPOCT} = \left(\frac{\sigma_2 l N_1^0 \sigma_1\lambda_{pu}P_{pu}}{2hc\pi r^2 f_0}\right)^2 P_{pr}. \tag{28}$$

The P_{PPOCT} of the other two schemes were derived in a similar manner and are provided in table 1.

It is illustrative to consider the theoretical P_{PPOCT} of the three schemes based upon relative values of the constants which go into the equations. In the limit $q_{2,3} \to 1$, where $q_{2,3}$ is the quantum efficiency for coupling states 2 and 3, and σ_2=σ_3, P_{PPOCT} for schemes 1 and 3 are equivalent. In the limit that σ_1=σ_2, P_{PPOCT} for schemes 1 and 2, differ by only a factor of 4 in favor of scheme 2. This factor of 4 arises from the fact that scheme 2 is sensitive to stimulated emission as well as absorption. In the limits noted, all three schemes have the potential to achieve comparable *SNR*. However, typically $q_{2,3}$<1 and σ_1>σ_2, which implies that in general scheme 2 will produce the best *SNR*. This may be illustrated by considering a real system, such as rhodamine 6G. It is possible to implement each of the three pump-probe schemes in rhodamine 6G. The relevant constants are σ_1=3.8x10^{-16} cm^2 (at 530 nm [30]), σ_2=0.7x10^{-16} cm^2 (at 1015 nm [32]), σ_3=0.59x10^{-16} cm^2 (at 580 nm [33]) , and $q_{2,3}$ = 0.008 [30]. The calculated P_{PPOCT} for schemes 1, 2, and 3 are then 1.90x10^{-10}, 6.25x10^{-8}, and 2.65x10^{-14}, respectively, which translate into *SNR* of 56 dB, 81 dB, and 17 dB. As expected, scheme 2 yields the best *SNR* of the three, however it is possible to find systems where this will not be the case. For instance, for systems which exhibit reverse saturable absorption (e.g. rhodamine B [34]), σ_2>σ_1, and for systems with highly perturbed spin states $q_{2,3}$ can become close to 1 (e.g. methylene blue [35]).

The validity of the above result for scheme 2 called ground state recovery PPOCT (gsrPPOCT) has been recently tested in reference [36]. The authors pumped and probed the first excited state of rhodamine 6G. They measured the *SNR* of a thin sample as a function of both the pump and probe power and found the functional dependence of both to quantitatively agree with that given in table 1.

Note that we do not discuss pump-probe schemes which work in the steady-state limit, because they have been discussed elsewhere[37, 38] and we can supply a physical reason why they should have inferior sensitivity than the non steady-state techniques described above. By its very definition, once the steady state is achieved the time rate of change of the molecular populations is zero, hence any pump radiation incident on the sample at that point provides no additional contrast. Since the PPOCT signal is always proportional to the population change induced by the pump, steady-state techniques waste pump photons by applying them to the sample when the probability of inducing a change in the population is zero. In contrast non steady-state techniques never reach the point of zero transition probability unless saturation of the excited state is achieved, which typically requires more power than would be available, limited by the tissue damage threshold.

#7900 - $15.00 USD Received 21 July 2005; revised 21 September 2005; accepted 23 September 2005

All of the nonlinear techniques would in principle benefit by a reduction in the pulse duration which implies a larger peak power accompanied by a broader pulse spectrum. Commercial sources are available that can routinely produce 20 fs pulses. Their use would lead to a 10 dB increase in SHOCT SNR and a 20 dB increase in NIVI and TPA-OCT SNR. Since NIVI (CARS) is a resonant process, the 20 dB increase may not be realized since the increased spectral bandwidth may not overlap with the bandwidth of the Raman transition. In principle the optimum transform limited pulse length for NIVI would result from a pulse duration which matched the natural lifetime of the Raman transition, thereby perfectly matching the spectral bandwidth of the Raman transition.

The signal of all MCOCT techniques is necessarily cumulative. For instance, consider a photon propagating through a tissue sample which has absorptive layers, where this absorption is being utilized as the contrast mechanism. When the photon traverses the absorptive layer it will be attenuated. If the photon is then immediately back scattered, the measurement of attenuation due to absorption will correctly identify the depth where the attenuation occurred. However, if the attenuated photon continues to propagate deeper into the tissue before being back scattered, it incorrectly identifies the depth where the attenuation occurred. This example is general to any of the techniques above which utilize absorption; SOCT, PPOCT, or TPA-OCT. A similar ambiguity arises in the non-referenced techniques SHOCT and NIVI. Instead of the photon being attenuated, it is created at some point in the tissue, however the position where it is back scattered is ambiguous. An algorithm needs to be applied to the raw MCOCT signal which removes this ambiguity. An algorithm has already been introduced in the literature specifically for SOCT[39] and PPOCT[37], however they are nearly identical and would work similarly for any technique which uses attenuation for contrast. An algorithm has not yet been established for either SHOCT or NIVI.

In order to simplify the appearance of the equations in table 1 we have neglected the attenuation of the sample arm light due to scattering in the sample for every technique except SOCT. For the other techniques we describe a simple algorithm to modify the equations of table 1 to account for attenuation due to single scattering and weak linear absorption by the sample. The power of any beam(s) is (are) attenuated at a rate of $P(z_g) = P' \exp\left(-\int_0^{z_g} \mu_s(\lambda) + \mu_a(\lambda) dz\right)$, where P' is the power incident on the surface of the sample, $P(z_g)$ is the power at depth z_g where the contrast signal is generated, $\mu_s(\lambda)$ is the samples scattering coefficient at wavelength λ, and $\mu_a(\lambda)$ is the samples absorption coefficient at wavelength λ. $P(z_g)$ should be inserted for all powers in the equations of table 1, except the SOCT equation. Furthermore, after the molecular contrast signal is generated P_{MCOCT} is attenuated at a similar rate of $P_{MCOCT}(z_R, z_g) = P'_{MCOCT}(z_g) \exp\left(-\left(\int_{z_g}^{z_R} \mu_s(\lambda) + \mu_a(\lambda) dz + \int_0^{z_R} \mu_s(\lambda)\mu_a(\lambda) dz\right)\right)$, where z_R is the depth at which the photons are reflected. The first integral is the attenuation from the generation depth to the reflection depth. The second integral is the attenuation from the reflection depth to the surface of the sample. We have also assumed that the molecular contrast signal is generated in the forward direction. Assuming it was generated in the backward direction simply changes the limits of integration.

While we have for the most part made comparisons of the *SNR* using constant molarity, in an attempt to follow as closely as possible the conventions for reporting sensitivity in the OCT literature, we could have fixed the *SNR* at 1 (0 dB) and reported the minimum detectable concentration. The latter metric is more commonly found in the microscopy literature. Since each technique has the same functional dependence on concentration, i.e. N^2, the relative results would be similar. The N^2 dependence of SHOCT and spectral triangulation are not obvious from table 1, however it is well known that $\chi^{(2)}$ is a linear

#7900 - $15.00 USD Received 21 July 2005; revised 21 September 2005; accepted 23 September 2005

function of N, hence eq. 8 is quadratic in N. Likewise, if we assume the weak absorber limit where the Taylor series expansion of the exponential function is a good approximation, eq. 17 simplifies to a function dependent on N^2. There is a then a simple relationship between the two metrics for all of the techniques discussed here. The following equation can be used to convert to minimum detectable concentration,

$$N_{md} = \sqrt{N^2 \Big/ 10^{SNR(dB)/10}} \tag{29}$$

where N_{md} is the minimum detectable concentration. The minimum detectable concentration for a technique with 80 dB *SNR* at 100 μM concentration is 10 nM under similar conditions. For convenience the final column of table 1 provides the minimum detectable concentration based upon equation 29 for each technique and contrast agent discussed.

4. Discussion

The first two techniques, SHOCT and NIVI are the only non-referenced techniques considered. While they have a clear fundamental *SNR* advantage over the referenced techniques as shown in Eqs. (1) and (2), their projected *SNR* is at best competitive, in the case of SHOCT and much worse in the case of NIVI than the referenced techniques. This is largely due to the fact that all of the referenced techniques exploit completely resonant molecular processes, which generally have much larger cross-sections than non-resonant processes. Hence, when considering the relative merits of one technique over another it is at least as important to consider the relative strength of the molecular process as whether the technique will be referenced of non-referenced.

The three referenced techniques all exploit absorption for molecular contrast. Of the three, spectroscopic OCT has been the most well studied. The major difficulty with the implementation of spectroscopic OCT is the separation of the attenuation of the sample arm power due to scattering from that due to absorption. The only detectible difference between the two is their different wavelength dependence. The wavelength dependence of absorption is typically highly peaked, while the wavelength dependence of scattering is much more slowly varying. Spectral resolution of the depth dependent intensity is required to exploit this difference, something not typically available in an OCT A-scan. For this reason, all spectral OCT variants split the spectral interference up into bands, such that the A-scan for each band has a different center wavelength. This results in a decrease in spatial resolution and *SNR*, the former because the effective bandwidth of the source for each wavelength dependent A-scan is smaller, the latter because the signal power is divided up between the wavelength dependent A-scans. The loss of spatial resolution and the fact that most absorption spectra in tissue are broad, makes spectroscopic OCT most well suited to very broad sources, similar to those that are finding use for ultra high resolution OCT. The difficulty of separating scattering from absorption has been the Achilles' heal of spectroscopic OCT, though recent advances, including spectral triangulation[28] and a spectral fitting algorithm[40] may pave the way for increased application of spectroscopic OCT for molecular imaging.

In contrast to spectroscopic OCT, the separation of absorption and scattering events in PPOCT is trivial. The modulation of the pump radiation shifts the PPOCT signal to a different frequency than the standard OCT signal. PPOCT also provides additional information by measuring excited state lifetimes, via the modulation of the pump-probe time delay. These attributes coupled to the zero loss in spatial resolution make gsrPPOCT a strong rival to spectroscopic OCT. The advantages of PPOCT are tempered by its more sophisticated setup, which requires at the very minimum a pulsed laser source and an electro- or acousto-optic modulator.

The absorption and scattering events are also easily separated in TPA-OCT, since the modulation of the sample arm power shifts the TPA signal to higher frequency. Like

#7900 - $15.00 USD Received 21 July 2005; revised 21 September 2005; accepted 23 September 2005

PPOCT, there is no inherent loss of spatial resolution in TPA-OCT. However, the projected *SNR* for TPA-OCT is significantly worse than either spectroscopic OCT or PPOCT. The major advantage of TPA-OCT is that it is easily done in the infrared with existing contrast agents. Most OCT work is done in the infrared because of the superior tissue penetration depth of infrared light. In contrast, both spectroscopic OCT and gsrPPOCT have a severe lack of suitable contrast agents in the infrared. This is largely a result of the fact that most contrast agents have been developed for use with fluorescence, which is rarer and generally much weaker in the infrared compared to the visible wavelengths. In spite of this advantage, TPA-OCT is likely only useful for the strongest two-photon absorbers, such as quantum dots.

Since all of the referenced techniques considered here exploit a resonant molecular process (absorption) in some way, it is in principle possible to develop derivative imaging techniques which will elucidate some of the biochemical dynamics of the system under study. There is a long history of using pump-probe techniques for this purpose in chemical and biochemical studies. Fluorescence microscopy makes use of techniques such as fluorescence return after photobleaching (FRAP) and fluorescence resonant energy transfer (FRET), to measure diffusion and make proximity measurements between fluorophores, respectively. The absorption analogs to these two techniques would garner complimentary information.

While we have concentrated on quantifying the sensitivity of the different techniques in this paper, as we noted in the introduction, the specificity of each technique is equally as important though less quantifiable. In general the specificity of a technique is linked to the number of physical properties it can measure, as well as the uniqueness of each property. For instance we can compare the measurement of vibrational and electronic transitions. In the condensed phase a high spectral resolution measurement of pure vibrational transitions is more specific than measuring an equivalent electronic transition, because in general the electronic transition will be severely broadened. The broadening of the electronic transition causes many different molecular species to have overlapping electronic spectra while the vibrational transitions remain fairly narrow. In addition, it is typically easier to measure multiple vibrational transitions generating what amounts to a fingerprint for a molecular species, than it is to measure multiple electronic transitions. To improve the specificity of electronic state measurements, the excited state lifetime may be measured as well as the excited state absorption lineshape, which may be structured.

5. Conclusions

In conclusion, we have considered the *SNR* ramifications for interferometric detection of molecular contrast signals that require a reference and those that require no reference. We found that the non-referenced interferometric techniques correspond approximately to dark field direct detection techniques and referenced techniques correspond approximately to the bright field direct detection techniques. Furthermore, the non-referenced techniques posses a fundamental *SNR* advantage over the referenced techniques, similar to the dark field advantage in direct detection.

We have derived the interferometric signal power for the molecular contrast techniques which have been reported in the literature, as well as techniques introduced here, two-photon absorption OCT and ground state recovery PPOCT, for the first time. While the non-referenced techniques, SHOCT and NIVI, posses a fundamental *SNR* advantage, the molecular processes which they exploit are so weak that the referenced techniques of spectral triangulation, PPOCT and TPA-OCT have larger signal powers than one or both. Of all of the techniques considered, spectral triangulation and gsrPPOCT emerge as the two most sensitive, with only 2 dB *SNR* difference between the two, when considered on a similar system. While spectral triangulation is most amenable to ultrabroadband sources, due to the inherent loss in spatial resolution and the need for a significant portion of an absorption peak

#7900 - $15.00 USD Received 21 July 2005; revised 21 September 2005; accepted 23 September 2005

in the spectral window, gsrPPOCT is capable of working with both ultrabroadband and normal bandwidth radiation sources.

Acknowledgments

We gratefully acknowledge support for this work through a grant from the National Institute of Health, R01 EB000243 and a Chandran research grant. BEA acknowledges support via a Kirschstein postdoctoral fellowship, F32 EB004237.

#7900 - $15.00 USD Received 21 July 2005; revised 21 September 2005; accepted 23 September 2005